

# Synthesis of Silver Nanoparticles Embedded Electrospun PAN Nanofiber Thin-Film Composite Forward Osmosis Membrane to Enhance Performance and Antimicrobial Activity

Shu-Fang Pan,<sup>‡,§,||</sup> Xiao-Xue Ke,<sup>‡,§</sup> Ting-Yu Wang,<sup>‡,§</sup> Qing Liu,<sup>‡,§</sup> Lu-Bin Zhong,<sup>‡</sup> and Yu-Ming Zheng<sup>\*,†,‡,§,||</sup>

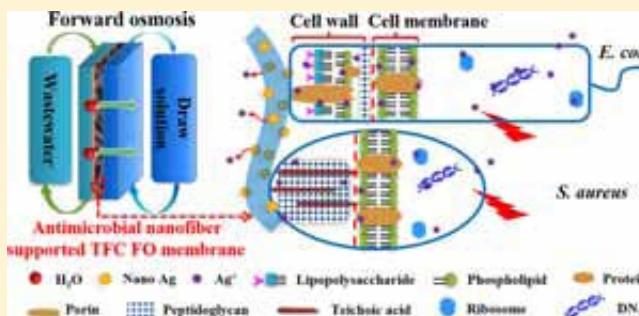
<sup>†</sup>CAS Center for Excellence in Regional Atmospheric Environment, Institute of Urban Environment, Chinese Academy of Sciences, Xiamen, Fujian 361021, China

<sup>‡</sup>CAS Key Laboratory of Urban Pollutant Conversion, Institute of Urban Environment, Chinese Academy of Sciences, Xiamen 361021, China

<sup>§</sup>University of Chinese Academy of Sciences, Beijing 100049, China

<sup>||</sup>Department of Analytical Science and Technology, Xiamen Huaxia University, Xiamen 361024, China

**ABSTRACT:** Enhancing antimicrobial activity is an effective strategy to mitigate membrane biofouling. In this study, an antimicrobial electrospun polyacrylonitrile (PAN) nanofiber mat decorated with in situ synthesized silver nanoparticles (AgNPs) was developed as support for a thin-film composite forward osmosis (FO) membrane. Effects of AgNPs on the physicochemical properties, water flux, reverse salt flux, and antimicrobial activity of the FO membrane were investigated, and also the antimicrobial mechanism was explored. Results showed AgNPs were monodisperse in the nanofibers, and the Ag/PAN nanofiber support (Ag/PAN-NFS) had a scaffold-like structure which could reduce internal concentration polarization. The Ag/PAN-NFS supported thin-film nanocomposite (Ag/PAN-TFN) FO membrane demonstrated outstanding hydrophilicity, resulting in high water fluxes in both FO and PRO modes. The Ag/PAN-TFN FO membranes, even the one with the lowest silver content of 0.5 wt %, exhibited excellent antibacterial activities for *E. coli* (96%) and *S. aureus* (92%), which was mainly due to the Ag<sup>+</sup>-species released into the solution.



## 1. INTRODUCTION

Global water and energy scarcities, two of the greatest crises, have been plaguing many countries around the world. It is reported that nearly two-thirds of the world's population lack of access to safe water,<sup>1</sup> and about 1.5 billion people live in electricity-deficient area.<sup>2</sup> It is urgent to exploit low-cost and effective methods for clean water production and energy generation. As an innovation in water treatment, membrane separation has gradually become one of the most promising water treatment technologies in the 21st century.<sup>3–5</sup> Recently, forward osmosis (FO) technology has drawn more and more attention,<sup>6–8</sup> which is a natural process that osmotic pressure difference supplies driving force and requires no or low external hydraulic pressure. Compared to reverse osmosis (RO) and nanofiltration (NF) membrane separation processes, FO displays a series of advantages such as low energy consumption, simple equipment, and higher water recovery.<sup>4,9</sup> Despite the aforementioned advantages, FO still suffers from the technical obstacle: lack of high efficiency membranes performing with high water flux, low internal concentration polarization (ICP), and antifouling property.<sup>10,11</sup>

Although fouling in FO was reported to be lower compared to NF and RO, it is still considered as a limitation for FO membrane performance, especially biofouling.<sup>12</sup> Biofouling is an inevitable and serious problem in the membrane separation process, leading to a reduction in water flux and severely affecting membrane lifetime. Essentially, biofouling is a kind of biofilm on the membrane surface, which starts from the attachment and growth of microorganisms.<sup>13</sup> Lately, thin-film composite (TFC) polyamide membranes are widely used in the FO process, which are susceptible to biofouling. Unlike conventional pressure-driven membranes, because of the absence of hydraulic pressure, FO membranes can be operated in FO mode (feed solution facing active layer) and PRO mode (feed solution facing porous support). Hence, the TFC membrane fouling takes place on the surface of active layer, outside and inside of support, and it is noteworthy that the fouling within porous structure is more severe and harder to

Received: October 5, 2018

Revised: December 12, 2018

Accepted: December 26, 2018

Published: December 26, 2018

clean.<sup>14</sup> For biofouling prevention and control in membrane separation processes, the key challenge is how to reduce the adhesion and viability of bacteria. Nevertheless, TFC membranes cannot tolerate common disinfectants, such as chlorine and its derivatives. As a result, new porous support needs to be developed to minimize the biofouling.

Lately, emerging electrospun nanofiber mats produced by electrospinning have showed great potential for many applications. Because of high porosity, large specific surface area, and interconnecting pore structures, the electrospun nanofiber mats have been explored for the applications in tissue engineering, catalysis, wastewater treatment, air filtration, and energy storage.<sup>15,16</sup> Recently, several studies have reported that the electrospun nanofiber mats can be successfully introduced as support for thin-film composite forward osmosis membranes.<sup>17,18</sup> In our previous work, we have successfully prepared self-sustained hydrophilic nanofiber support for TFC FO membrane.<sup>18</sup> Due to the special scaffold-like structure, the nanofiber support can effectively mitigate the ICP, improving water flux. However, this support is still subjected to biofouling, and to the best of our knowledge, no antimicrobial nanofiber support was developed and employed in the FO membrane preparation.

On the other hand, bactericides or antibacterial materials such as nanoparticles can be decorated on/within the nanofibers for antimicrobial applications. Silver nanoparticles (AgNPs), a very promising antimicrobial agent, have been incorporated in nanofibers, which have gained particular attentions such as water filtration<sup>19</sup> and wound dressings.<sup>20</sup> In addition, AgNPs have been introduced into membrane materials for biofouling mitigation via phase-inversion,<sup>21</sup> layer-by-layer assembly,<sup>22</sup> and membrane surface modification.<sup>23</sup> Due to a very effective activity against a broad range of microorganisms,<sup>24</sup> these membranes displayed improved antibiofouling activity. Furthermore, the incorporation of AgNPs can increase the surface hydrophilicity of membranes, leading to a higher water flux and a better antimicrobial activity.<sup>22</sup> Therefore, aiming at improving water flux as well as reducing biofouling and ICP, a composite electrospun nanofiber mat containing AgNPs is expected to be a promising material as antibiofouling support for thin-film composite forward osmosis membrane.

Herein, we aim to synthesize an antimicrobial silver/polyacrylonitrile (Ag/PAN) nanofiber mat as support for the TFC FO membrane. Although AgNPs is an ideal antibacterial material, there is still a challenge to prevent their aggregation to get a good dispersion in the nanofibers. So, in this study, a facile method of in situ synthesis of AgNPs on/within nanofibers was developed, which can effectively keep the AgNPs from aggregation. PAN was chosen as polymeric matrix because of its good electrospinnability and high tensile strength after electrospinning. More importantly, PAN is an ideal carrier of silver ion, making it a prominent support for in situ synthesis of AgNPs.<sup>25</sup>

Figure 1 illustrates the preparation of a Ag/PAN nanofiber thin-film nanocomposite (Ag/PAN-TFN) FO membrane. In brief, the AgNO<sub>3</sub>/PAN nanofiber mat was first prepared via electrospinning technique. The AgNO<sub>3</sub>/PAN nanofiber mat was then laminated, followed by immersing in N<sub>2</sub>H<sub>4</sub>·H<sub>2</sub>O solution to reduce Ag<sup>+</sup> into Ag<sup>0</sup> in situ. After that, a thin PA layer was deposited on the Ag/PAN nanofiber support (Ag/PAN-NFS) via interfacial polymerization to obtain an antimicrobial Ag/PAN-TFN FO membrane. Also, in this

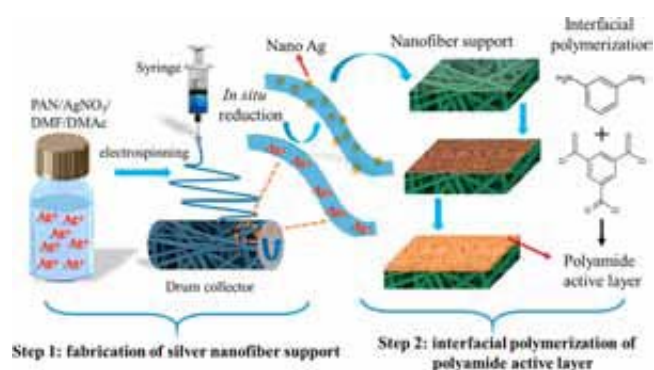


**Figure 1.** Schematic diagram of the preparation of the silver/polyacrylonitrile nanofiber thin-film nanocomposite (Ag/PAN-TFN) FO membranes.

work, the scanning electron microscope (SEM), transmittance electron microscopy (TEM), X-ray diffraction (XRD) and X-ray photoelectron spectroscopy (XPS) were used to characterize the morphology and structure of the Ag/PAN-NFS. Furthermore, the effects of silver contents (0, 0.5, 1, 2 wt % to PAN) on the Ag/PAN-TFN FO membrane osmosis performance, silver leaching behavior and antimicrobial properties were systematically investigated.

## 2. MATERIALS AND METHODS

**2.1. Materials.** Polyacrylonitrile (PAN, Mw = 90 000 g/mol) was purchased from Kunshan Hongyu Plastic Co., Ltd. *N,N*-Dimethylformamide (DMF), *N,N*-dimethylacetamide (DMAc), and hydrazine hydrate (N<sub>2</sub>H<sub>4</sub>·H<sub>2</sub>O) were obtained from Sinopharm Chemical Reagent Co., Ltd. *m*-Phenylenediamine (MPD) and 1,3,5-trimesoyl chloride (TMC) were purchased from Sigma-Aldrich. Silver nitrate (AgNO<sub>3</sub>) was purchased from Shanghai Shenbo Chemical, Co., Ltd. Hexane was received from Xiya Reagent. Commercial asymmetric cellulose triacetate (HTI-CTA), and thin-film composite (HTI-TFC) FO membranes were acquired from Hydration Technology Innovations Inc. (Albany, OR). The ultrapure water (18.2 MΩ) used in all experiments was obtained from a Milli-Q system (Millipore, Massachusetts).

**2.2. Preparation of the Ag/PAN-TFN FO Membrane.** DMF and DMAc were mixed by the weight ratio of 1:1 as mixed solvent. PAN was added into the mixed solvent and stirred at 60 °C for 5 h to obtain homogeneous PAN solution of 10 wt %. Silver nitrate was then added into the as-prepared PAN solution, and the loading levels were 0, 0.5, 1, and 2 wt % with respect to the weight of PAN (Table 1). The resultant solution was stirred for 12 h at room temperature to dissolve the silver nitrate completely. Subsequently, the as-prepared AgNO<sub>3</sub>/PAN solution was used as spinning solution, which was then electrospun onto an aluminum foil with a voltage of 15 kV to form a nanofiber mat. Feeding rate of the spinning solution was 0.9 mL/h, and the tip-to-collector distance was 15 cm.

The as-prepared AgNO<sub>3</sub>/PAN nanofiber mat was laminated with a paper laminator (no. 3893, Deli, China), which was then immersed into a 0.8 M N<sub>2</sub>H<sub>4</sub>·H<sub>2</sub>O solution to reduce the Ag<sup>+</sup> ions in the nanofiber into Ag<sup>0</sup> in situ. The obtained Ag/PAN nanofiber support containing AgNPs was rinsed with 50% alcohol solution, which was subsequently used for the fabrication of Ag/PAN-TFN FO membrane.

**Table 1. Composition of the Different Electrospinning Solutions to Prepare the Silver Nanofiber Support (Ag/PAN-NFS)**

sample	abbreviation	PAN (wt %)	DMF:DMAc (w:w)	AgNO <sub>3</sub> (wt %, by weight of PAN)
pristine	pristine	10	1:1	0
0.5Ag/PAN-NFS	0.5Ag-NFS	10	1:1	0.5
1Ag/PAN-NFS	1Ag-NFS	10	1:1	1
2Ag/PAN-NFS	2Ag-NFS	10	1:1	2

A thin polyamide (PA) active layer was deposited on the Ag/PAN-NFS by interfacial polymerization to fabricate the Ag/PAN-TFN FO membrane. Briefly, the Ag/PAN-NFS was first immersed in a 3% (w/v) MPD aqueous solution for 2 min. After that, the Ag/PAN-NFS was taken out, and the excess MPD solution was removed from the surface by tissue papers. Then, the Ag/PAN-NFS was fixed by a dual-tier frame, and the top surface of the Ag/PAN-NFS was contacted with a 0.2% (w/v) TMC hexane solution for 1 min to form an ultrathin polyamide film via the interfacial polymerization between MPD and TMC. The freshly prepared Ag/PAN-TFN FO membrane was cured in a vacuum oven at 80 °C for 10 min, followed by immersing in deionization (DI) water at 4 °C for 12 h. The Ag/PAN-TFN FO membranes with different Ag contents (0, 0.5, 1, and 2 wt %) were abbreviated as pristine-TFN, 0.5Ag-TFN, 1Ag-TFN, and 2Ag-TFN, respectively.

**2.3. Characterization of the Ag/PAN-TFN FO Membrane.** The morphology of the Ag/PAN-NFS and the Ag/PAN-TFN FO membrane were observed with a field emission scanning electron microscope (FESEM, S-4800, HITACHI, Japan) operated at 5 kV. Before imaging, samples were sputter coated with a thin layer of gold to achieve better contrast. For cross-sectional imaging, the samples were freeze-cracked using liquid nitrogen to obtain a clean edge. TEM photographs of the samples were conducted on a HITACHI H-7650 system (Japan). XRD graphs were obtained using a PANalytical X'Pert PRO (Almelo, Netherlands), and the range of diffraction angle ( $2\theta$ ) of 10–90° was used. Due to that the diffraction peaks of samples with low silver content cannot be detected by XRD, so Ag/PAN-NFS with 10 wt % silver was chosen for XRD detection.

A contact angle analyzer (DSA 100, KRUSS, Germany) was used to characterize water contact angles on the Ag/PAN-NFS surfaces by a sessile drop method. Before testing, the samples were dried at 60 °C and stored in a dryer. Video mode was applied to record the changes of water droplet on the surfaces. The volume of tiny droplet was kept at 3  $\mu$ L, and the contact angle values were measured at 1, 2, and 5 s after the water drop contacting with the surface.

The chemical structure information on the Ag/PAN-NFS and Ag/PAN-TFN FO membrane were obtained from a Fourier transform infrared spectroscopy (FTIR, iS10, Thermo, U.S.A.) with a transmission mode. The spectra were recorded between 400 and 4000  $\text{cm}^{-1}$  with a scan number of 32.

XPS spectra of the AgNO<sub>3</sub>/PAN nanofiber and the Ag/PAN-NFS were collected using a PHI Quantum-2000 electron spectrometer (Ulvac-Phi, Japan) with 150 W monochromatized Al K $\alpha$  radiation (1486.6 eV). A binding energy (BE) range of 0–1320 eV was used for wide scan XPS spectra, and step sizes of 0.8 and 0.125 eV were set for wide scan and high-resolution scan spectra, respectively. The carbon 1s electron BE (284.8 eV) corresponding to graphitic carbon was used to calibrate the scan spectra.

**2.4. Evaluation of the Ag/PAN-TFN FO Membrane Performance.** The performance of FO membrane was

evaluated with a lab-scale cross-flow FO system equipped with a cross-flow membrane cell (effective area 40  $\text{cm}^2$ ) in both FO and PRO modes. Then 2 L of draw solution (0.5 M NaCl) and 2 L of feed solution (DI water) flowed counter on each side of the membrane. The feed and draw solutions were circulated with peristaltic pumps (WT600, Longer, China) at a flow rate of 600 mL/min (12.5 cm/s). The temperatures of the feed and draw solutions were kept at 25 °C.

The water flux ( $J_w$ ,  $\text{L m}^{-2} \text{h}^{-1}$ , abbreviated as LMH) and reverse salt flux ( $J_s$ ,  $\text{g m}^{-2} \text{h}^{-1}$ , abbreviated as gMH) were determined as follows:

$$J_w = \frac{\Delta V}{s\Delta t} \quad (1)$$

$$J_s = \frac{c_F V_F - c_{F,i} V_{F,i}}{s\Delta t} \quad (2)$$

where  $\Delta V$  (L) is the volume of permeation water collected in a predetermined time  $\Delta t$  (h) during the test and  $s$  is the area of effective membrane surface ( $\text{m}^2$ ).  $C_F$  (g/L) and  $V_F$  (L) are the salt concentration and total volume of the feed at the end of test, respectively. While  $C_{F,i}$  (g/L) and  $V_{F,i}$  (L) refer to the initial salt concentration and total volume at the beginning of tests, respectively. All performance results were obtained from three replicate tests.

**2.5. Antimicrobial Activity of the Ag/PAN-TFN FO Membrane.** **2.5.1. Silver Leaching Test.** To quantify the possible release of silver ions from the Ag/PAN-TFN FO membrane, a piece of membrane with a dimension of 1.0 cm  $\times$  3.0 cm was immersed into 10 mL of DI water under shaking condition at room temperature. After a predetermined interval, the membrane was transferred into another 10 mL of fresh Milli-Q water. The concentration of silver ion released into the water was measured by an inductively coupled plasma mass spectrometer (ICP-MS, Agilent, model 7500CX). The leaching tests were conducted for 32 days in triplicate.

Further, to determine the silver concentration in solution of FO processes with different Ag/PAN-TFN FO membranes, the following equations were applied:

$$C_{\text{Ag}} = \frac{r_{\text{Ag}}st}{V_{D,i} + \Delta V} \quad (\text{in FO mode}) \quad (3)$$

$$C_{\text{Ag}} = \frac{r_{\text{Ag}}st}{V_{F,i} - \Delta V} \quad (\text{in PRO mode}) \quad (4)$$

where  $r_{\text{Ag}}$  ( $\mu\text{g cm}^{-2} \text{day}^{-1}$ ) was the average releasing rate of silver ions between the day 12 and day 32 (after 12 days, the rate of silver ion release became stable),  $t$  (h) was the experiment time in both modes, and  $V_{D,i}$  (L) represented initial volume of the draw solution.

**2.5.2. Diffusion Inhibition Zone Test.** The antimicrobial properties of the Ag/PAN-TFN FO membranes were assessed using two model bacteria: Gram-negative *Escherichia coli* (*E. coli*) and Gram-positive *Staphylococcus aureus* (*S. aureus*). *E.*

*coli* (CMCC 44103) was obtained from Guangdong Microbiology Culture Center (Guangdong, China), and *S. aureus* was kindly provided by Prof. Xin Yu from the Institute of Urban Environment, Chinese Academy of Sciences (Xiamen, China).

Diffusion inhibition zone test of the Ag/PAN-TFN FO membranes was performed according to the method reported elsewhere.<sup>22</sup> Both cultures were grown in a LB broth at 37 °C overnight, and overnight bacterial cultures were cultured in a fresh LB broth for 2–3 h to exponential phase. The resultant culture with a volume of 100  $\mu\text{L}$  was spread on a LB agar plate, on which a pristine Ag/PAN-TFN FO membrane disc with a diameter of 21 mm were placed after ultraviolet sterilization. Then the agar plate was incubated at 37 °C for 24 h to form the diffusion inhibition zone, which was then photographed by using a digital camera. Further more, to study the effect of silver ion release on the antimicrobial property, the antibacterial activity of the Ag/PAN-TFN FO membranes after immersing in ultrapure water for 30 days at room temperature was also evaluated by the method of diffusion inhibition zone.

**2.5.3. Cell Viability Analysis.** Viable cell attachment tests were employed to analyze the number of live bacteria attached to the Ag/PAN-TFN FO membrane. A 2–3 h bacterial culture was centrifuged for 10 min at 2700 rpm to remove the LB broth, and the bacteria were suspended in 0.9% sterile saline to form a concentration of  $\sim 10 \times 10^7$  cells/mL. Square support samples (4  $\text{cm}^2$ ) were immersed in the bacterial suspension at 37 °C for 1 h. The samples were then taken out and washed gently with a 0.9% sterile saline to remove the bacteria that did not adhere firmly. Subsequently, the support was put into 10 mL of sterile saline, followed by 7 min sonication to release the cells. The suspension was then serially diluted, plated on LB agar plates, and incubated at 37 °C overnight to count the colonies. All tests were performed in triplicate.

Additionally, to observe changes of cell morphology after contacting with the Ag/PAN-TFN FO membrane, the samples were fixed with 5% glutaraldehyde and dehydrated with serial ethanol, followed by imaging with SEM.

### 3. RESULTS AND DISCUSSION

**3.1. Characterization of the Ag/PAN-NFS and the Ag/PAN-TFN FO Membrane.** Figure 2 shows the SEM micrographs and fiber diameter distribution of the silver/polyacrylonitrile nanofiber support (Ag/PAN-NFS) with different contents of AgNPs. For all of the nanofiber mats, uniform and smooth nanofibers were obtained. Notably, the Ag/PAN-NFS were fully porous with interconnecting pores, which can favor the mass transfer, leading to a lower ICP.<sup>26</sup> When the silver nanoparticle was introduced into the PAN nanofiber, the fiber diameter (0.5Ag-NFS) became larger and then gradually decreased with a higher content of silver nanoparticle. This is the result from the change of viscosity and conductivity of electrospinning solution. When  $\text{AgNO}_3$  was added into the electrospinning solution, both the viscosity and conductivity of PAN solution increased. The increased viscosity resulted in a larger fiber diameter, whereas the increased conductivity led to a smaller one.<sup>27</sup> With the increment of silver ion content, the conductivity played a more important role in fiber diameter.

However, no AgNPs were observed in SEM images, which may be due to the low silver contents or the small size of silver nanoparticles. In order to verify the presence of AgNPs in the

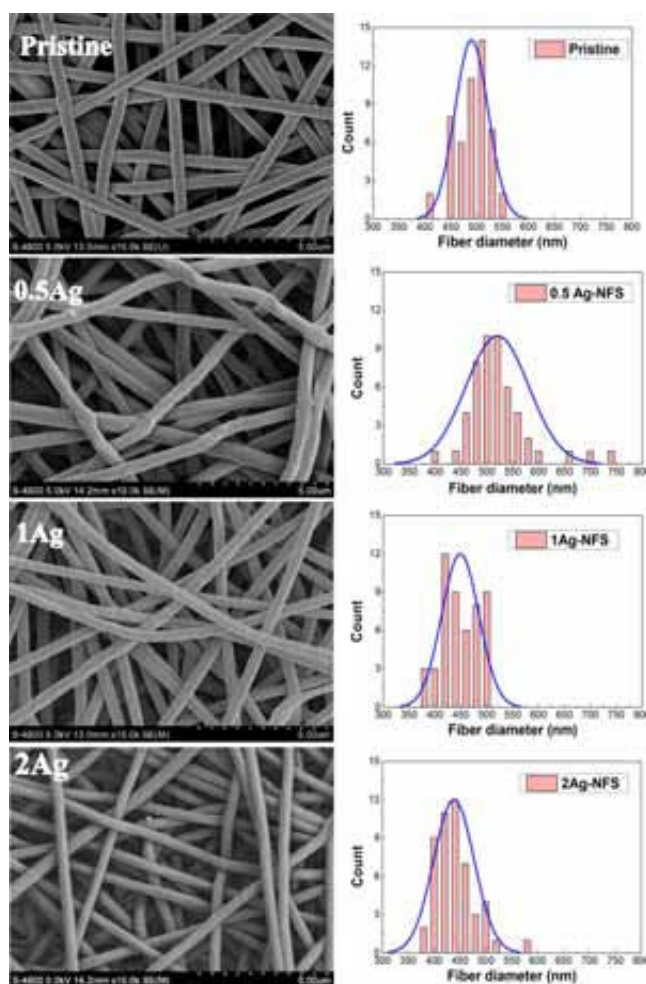


**Figure 2.** SEM micrographs and fiber diameter distribution of the silver/polyacrylonitrile nanofiber support (Ag/PAN-NFS) with different contents of AgNPs. The average diameters were  $490 \pm 32$ ,  $520 \pm 61$ ,  $449 \pm 36$ , and  $438 \pm 39$  nm for the pristine, 0.5Ag, 1Ag, and 2Ag PAN nanofiber support, respectively.

PAN nanofiber, the TEM micrograph was captured (Figure 3a). It was observed that AgNPs with a size about 10 nm were uniformly distributed on/within the PAN nanofibers without any aggregations. The monodispersed AgNPs was mainly attributed to that cyano groups in PAN can immobilize the silver ions through coordination bond.<sup>25</sup> In addition, XRD spectra were acquired to identify the phase structure of the Ag/

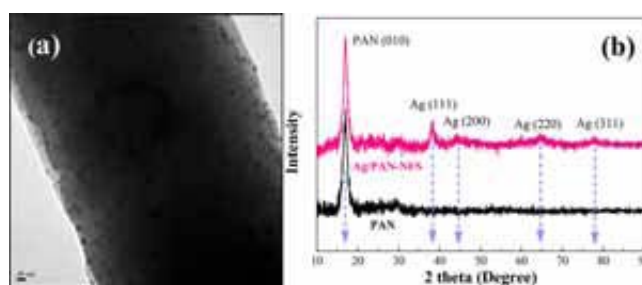


**Figure 3.** (a) TEM image of Ag/PAN-NFS and (b) XRD patterns of PAN and Ag/PAN-NFS. In order to better characterize the morphology of AgNPs, the NFSs with higher content of silver, 2Ag-NFS and 10Ag-NFS, were prepared for TEM and XRD, respectively.

PAN-NFS (Figure 3b). It was observed that the diffraction peak at  $16.9^\circ$  ( $2\theta$ ) in both Ag/PAN-NFS and pure PAN nanofibers was corresponding to the (010) plane of PAN (PDF no. 048-2119). The Ag/PAN-NFS possessed four extra  $2\theta$  peaks at  $38.2^\circ$ ,  $44.3^\circ$ ,  $64.4^\circ$  and  $77.5^\circ$ , corresponding to the (111), (200), (220), and (311) planes of cubic phase Ag (PDF no. 004-0783). The results of TEM and XRD showed the successful incorporation of AgNPs.

XPS analysis of Ag/PAN-NFS before and after in situ reduction was carried out to further explore the elemental composition of the support. Figure 4a gives the wide scan XPS spectra in the binding energy range 200–600 eV. Other than the peaks corresponding to C 1s, N 1s, and O 1s, the Ag 3d region was observed in both spectra of NFS before and after in situ reduction of Ag, indicating the successful incorporation of

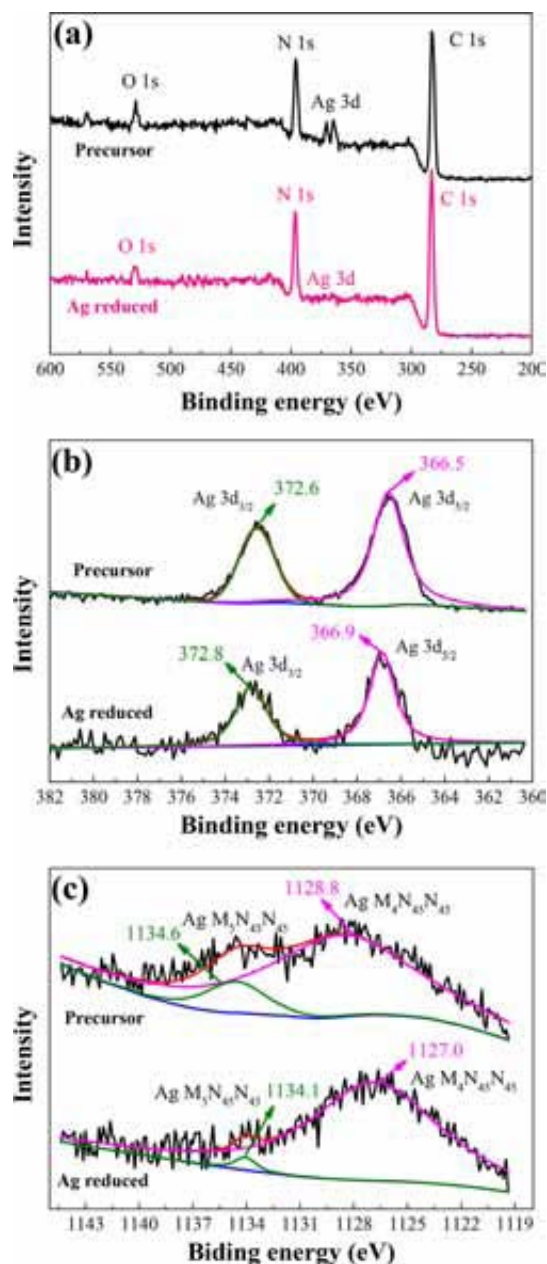


**Figure 4.** (a) XPS wide-scan spectra, (b) high resolution Ag 3d XPS spectra, and (c) Ag Auger spectra of the precursor and reduced 2Ag/PAN-NFS, respectively.

silver in the nanofibers. High resolution XPS spectra of Ag 3d of both samples displayed in Figure 4b were doublets with energy difference of 6.0 eV. Some studies reported an anomalous negative shift in BE of Ag 3d peaks for oxidation states,<sup>28</sup> which were basically consistent with our results (Figure 4b). After reduction reaction, the peak of Ag 3d<sub>5/2</sub> shifted from 366.5 (precursor) to 366.9 eV and the peak of Ag 3d<sub>3/2</sub> slightly shifted from 372.6 (precursor) to 372.8 eV. This increase of BE of Ag 3d peaks indicated the reduction of Ag ions, which was further confirmed by the Ag Auger spectra in Figure 4c. It is considered to be more reliable that use of the Auger spectra identifies silver oxidation states.<sup>29</sup> The peaks of Ag M<sub>5</sub>N<sub>45</sub>N<sub>45</sub> and Ag M<sub>4</sub>N<sub>45</sub>N<sub>45</sub> in the precursor were located at 1134.6 and 1128.8 eV, respectively. The negative BE shifts of Ag MNN peaks, in particular for Ag M<sub>4</sub>N<sub>45</sub>N<sub>45</sub> (from 1128.8 to 1127.0 eV), were obviously observed after the Ag reduction. This confirmed that the Ag<sup>+</sup> was in situ reduced to Ag<sup>0</sup> by the hydrazine hydrate.

To characterize the changes of hydrophilicity of the nanofiber support with different Ag contents, the water contact angle was measured. With the adding of silver, water droplet on the top surface of the support could be quickly absorbed by the nanofibers. Thus, the contact angle of Ag/PAN-NFS was rapidly reduced to zero in five seconds, especially for 1Ag-NFS and 2Ag-NFS (Figure 5). The higher hydrophilicity of the

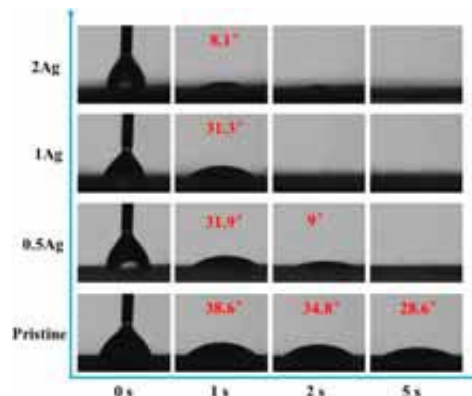


**Figure 5.** Water contact angles of the Ag/PAN-TFN FO membranes with different silver contents as a function of time after the water drop contacting with the surface.

support facilitated the stronger affinity to water, subsequently leading to better mass transfer and enhancing the water flux.<sup>30</sup> In addition, the more hydrophilic surfaces reduces bacterial adhesion and organic fouling like protein.

The morphology of Ag/PAN-TFN FO membrane is exhibited in Figure 6. The thickness of the membrane was about 70  $\mu\text{m}$  determined by measuring the cross-section microimage (Figure 6a). In Figure 6b, it can be seen that the membrane consists of a thin active layer and a scaffold-like support which could favor the mass transfer of water and salts. The PA active layer, as shown in Figure 6c, fully covered the top surface of the porous nanofiber support, endowing a typical ridge-valley structure via interfacial polymerization. In order to confirm the formation of PA layer, FTIR spectra of the Ag/PAN-NFS and corresponding Ag/PAN-TFN FO membrane were displayed in Figure 6d. The apparent absorption peaks at  $1540\text{ cm}^{-1}$  ( $-\text{N}-\text{H}$ , amide II peak) and  $1663\text{ cm}^{-1}$  ( $-\text{C}=\text{O}$ , amide I peak) were observed in the spectra of Ag/PAN-TFN FO membrane, and the peak at  $1611\text{ cm}^{-1}$  was resulted from

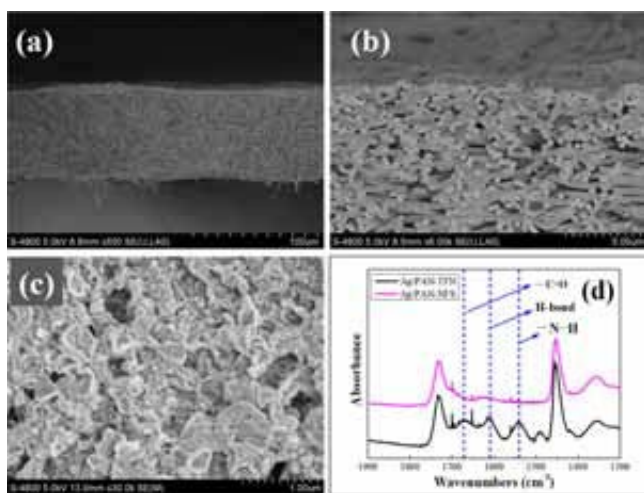


**Figure 6.** (a) Cross-section microimage, (b) the enlarged cross-section microimage and (c) the top layer morphology of the Ag/PAN-TFN FO membranes; (d) FTIR spectra of Ag/PAN-TFN and corresponding Ag/PAN-TFN FO membrane.

the aromatic ring breathing. This indicated the successful deposition of polyamide active layer on support.

### 3.2. Performance of the Ag/PAN-TFN FO Membrane.

**3.2.1. Osmotic Flux Performance of the Ag/PAN-TFN FO Membrane.** The behavior and performance of the Ag/PAN-TFN FO membranes and two commercial FO membranes (HTI-CTA, HTI-TFC) were displayed in Figure 7. All of the

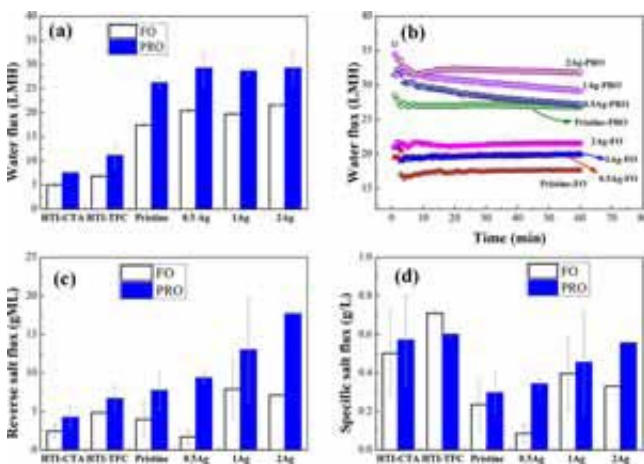


**Figure 7.** (a) Water flux of the Ag/PAN-TFN and commercial FO membranes and (b) water flux behavior of the Ag/PAN-TFN FO membranes as a function of time operated in FO and PRO modes. (c) Reverse salt flux and (d) specific salt flux of the Ag/PAN-TFN and commercial FO membranes operated in FO and PRO modes. Experimental conditions: draw solution = 0.5 M NaCl; DI water used as feed solution; FO mode: active layer facing feed solution; PRO mode: active layer facing draw solution.

membranes operated in PRO mode presented much higher water flux than that in FO mode. This is mainly due to the fact that the concentrative ICP in PRO mode results in a higher effective osmotic pressure difference than the dilutive ICP in FO mode.<sup>31</sup> Moreover, it was found that water flux of Ag/PAN-TFN FO membranes is much higher than that of commercial FO membranes in both modes. The Ag/PAN-TFN FO membranes yielded about 3-fold and 4-fold higher

water flux performance as compared to HTI-TFC and HTI-CTA FO membranes, respectively (Figure 7a). This was mainly attributed to the hydrophilic scaffold-like support with interconnected pores, which facilitates a better mass transfer of the Ag/PAN-TFN FO membrane than that of the phase-inversion support of HTI-TFC and HTI-CTA FO membranes. So the Ag/PAN-TFN FO membrane presented a much lower ICP and had a higher water flux. Compared with the pristine membranes (nanofiber support without AgNPs), a flux ascent in the Ag/PAN-TFN FO membranes resulted from the more hydrophilic supports with the embedded AgNPs, which was in agreement with the results from water contact angle analysis. Thus, by using 0.5 M NaCl as the draw solution, the 2Ag-TFN possessed high water fluxes of 21.58 LMH and 29.21 LMH in FO and PRO mode, respectively.

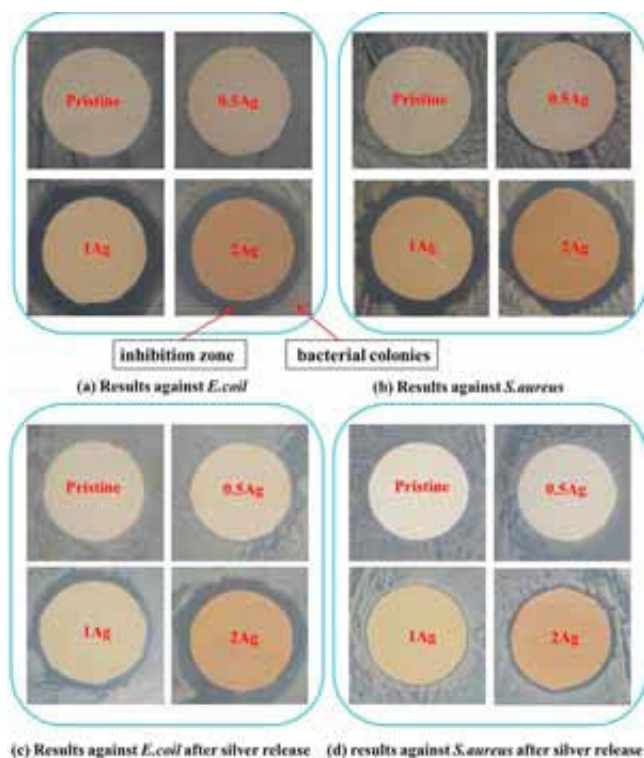
The water flux of Ag/PAN-TFN FO membrane as a function of time is shown in Figure 7b. All of the membrane exhibited comparably stable water flux in FO mode, while there is an obvious decline in PRO mode. The major reason is that the larger water flux diluted the draw solution and then further resulted in a decrease of effective osmotic pressure difference.

Figure 7c,d show the reverse salt flux and the specific reverse salt flux, respectively. Reverse salt flux is the amount of draw solute permeates into the feed solution per unit volume, while the specific reverse salt flux is the value of  $J_s/J_w$ , which means loss of draw solute per unit of water produced. When different membranes and/or experimental conditions were utilized, the specific reverse salt flux was employed to evaluate the overall membrane performance. Compared to the commercial FO membranes, the Ag/PAN-TFN membranes suffered from a relative higher reverse salt flux in both modes (Figure 7c). However, in terms of the specific reverse salt flux as shown in Figure 7d, the Ag/PAN-TFN membranes exhibited much lower values in both FO and PRO modes. A lower specific reverse salt flux of the Ag/PAN-TFN FO membrane reflected an increase in the selectivity of membrane and a higher efficiency of the FO process.

On the other hand, all the Ag/PAN-TFN and pristine FO membranes displayed lower  $J_s$  in FO mode versus PRO mode. The trade off in water flux and salt flux could attribute this phenomenon. Obviously, it was found that the salt flux of 2Ag/PAN-TFN FO membrane respectively increased by 78% and 130% with respect to pristine PAN-TFN FO membrane in FO and PRO mode. The significant increment in reverse salt flux might result from that the PA active layer was more prone to breakage, which could be caused by the swelling of 2Ag-NFS with excellent hydrophilicity.<sup>32,33</sup> The hydrophilicity of support can affect the structure and performance of polyamide, and a more hydrophilic support can result in a higher salt flux, which was discussed in our previous work.<sup>18</sup> As shown in Figure 7d, a remarkably high specific salt flux was observed in both modes for the 2Ag/PAN-TFN FO membrane. This was corresponding to the behavior of reverse salt flux, indicating that a higher silver content in support could affect the property of PA active layer.

**3.2.2. Antimicrobial Activity of the Ag/PAN-TFN FO Membranes.** **3.2.2.1. Inhibition Zone.** An inhibition zone is a transparent circle around the sample, in which the bacteria is inhibited by the diffusion of the antibacterial material in the agar plate. Diffusion inhibition zones around the Ag/PAN-TFN FO membranes were observed to evaluate their antimicrobial activities against two commonly used model

bacteria, *E. coli* and *S. aureus* (Figure 8). As shown in Figure 8a,b, clear inhibition zones around the 1Ag-TFN and 2Ag-TFN



**Figure 8.** Antibacterial activity of Ag/PAN-TFN membranes against *E. coli* and *S. aureus* in the disc diffusion test. The membrane discs used in panels c and d had been immersed into ultrapure water to release silver statically for 30 days before test.

TFN FO membranes indicated their excellent antimicrobial capacity against both *E. coli* and *S. aureus*. As for the 0.5Ag-TFN FO membrane, the inhibition zones were not obvious, while the pristine membrane did not perform any inhibition efficiency toward both the cultures. The above results indicated that the antibacterial efficiency of Ag/PAN-TFN FO membranes was induced by the embedded silver nanoparticles. Although the antibacterial mechanism of AgNPs was not clearly explained,<sup>24</sup> the formation of inhibition zones was possibly ascribed to the silver ions releasing into the LB medium from the Ag/PAN-NFS.

In addition, the inhibition zones around the membranes that have released silver for 30 days are displayed in Figure 8c,d. The 1Ag/PAN-TFN and 2Ag/PAN-TFN FO membranes still possessed the significant antimicrobial capability, and as the silver content was higher, the inhibition zone was clearer and wider. Moreover, the Ag/PAN-TFN FO membranes showed greater effectiveness in restraining the growth of *E. coli* than *S. aureus*. The probable reason for this phenomenon was discussed in the following parts.

**3.2.2.2. Cell Viability.** Figure 9 depicts the attached live fractions of *E. coli* and *S. aureus* cells on support after contacting with bacteria suspension. The quantitative analysis showed a strong antimicrobial activity of the Ag/PAN-NFS containing AgNPs. After 1 h contact, the amount of viable *E. coli* and *S. aureus* decreased sharply with the increasing silver content. These reductions in the number of viable adherent bacteria on the Ag/PAN-NFS were significantly different from the pristine membranes with *p*-values of less than 0.03 for both

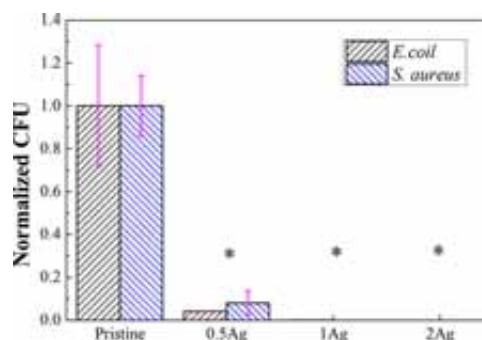


**Figure 9.** Viable adherent fractions of *E. coli* and *S. aureus* cells in sterile saline ( $\sim 10^7$  cells/mL) in contact with the Ag/PAN-TFN FO membrane at 37 °C for 1 h. Asterisks (\*) indicated a statistically significant difference between the Ag-TFN and pristine support ( $p < 0.03$ ).

model bacteria. It is worth noting that there were hardly any viable cells detected on the 1Ag-NFS and 2Ag-NFS, and relative to the PAN-NFS without AgNPs, the 0.5Ag-NFS exhibited antibacterial activity of 96% and 92% for the *E. coli* and *S. aureus*, respectively.

This significant difference in viable adherent fractions resulted from the biotoxicity of the incorporated AgNPs. SEM micrographs of bacteria morphology on the PAN-NFS and Ag/PAN-NFS are shown in Figure 10, which validated the

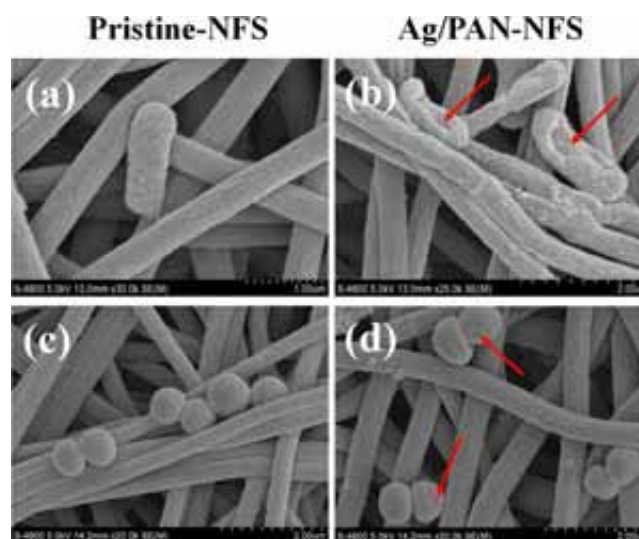


**Figure 10.** SEM micrographs of the bacteria morphology for *E. coli* on (a) nanofiber support without AgNPs (pristine-NFS) and (b) PAN nanofiber with AgNPs (Ag/PAN-NFS) and for *S. aureus* on (c) pristine-NFS and (d) Ag/PAN-NFS. The red arrows were used to point out the “pits” on bacteria.

biotoxicity of AgNPs. Compared to the cells attached to the pristine membranes, most the cells adhered on Ag/PAN-NFS exhibited the “pits”, and the morphology change was more obvious on the cells of *E. coli* than *S. aureus*. It was mainly due to the structure difference of cell wall between Gram-negative and Gram-positive bacteria.

*S. aureus*, a typical Gram-positive microbe, has a thick cell wall consisting of peptidoglycan and teichoic acid, while the wall thickness of the Gram-negative *E. coli* was much smaller with complex multilayer including the lipopolysaccharide, phospholipid, peptidoglycan, and some membrane protein.<sup>34</sup>

The cell wall of *S. aureus* has a much thicker peptidoglycan layer than that of *E. coli*. The thicker peptidoglycan cell wall imparts a much stronger defense system to the *S. aureus*, which could prevent AgNPs and silver ions penetrating through the bacterial cell wall.<sup>34</sup> The morphology distinction between the *E. coli* and the *S. aureus* cells may be the main reason for the less antibacterial activity of the Ag/PAN-NFS FO membrane against *S. aureus* in tests of diffusion inhibition zone and cell viability.

**3.3. Antimicrobial Mechanism and Antibiofouling Potential of the Ag/PAN-TFN FO Membrane.** As mentioned above, the antimicrobial activity of the Ag/PAN-TFN FO membrane was attributed to the broad-spectrum antibacterial activity of AgNPs. Recently, some studies have proposed that the mechanism of antibacterial action of AgNPs is driven by the generation of reactive oxygen species (ROS) by the AgNPs attached to the bacteria,<sup>35</sup> while some ascribed the antibacterial activity to the Ag<sup>+</sup>-species released from the oxidative dissolution of nanoparticles.<sup>24</sup> In this work, as immobilized in the PAN nanofibers, most of the AgNPs could not directly contact with the bacteria. Therefore, we considered that the preponderant antibacterial activity of the Ag/PAN-TFN FO membranes was due to the Ag<sup>+</sup>-species released from the nanofiber support embedded with AgNPs. So in order to verify the possible release of silver ions, leaching tests were analyzed using ICP-MS.

Figure 11a depicts the dynamic releasing rate of silver ions into water from the Ag/PAN-TFN FO membrane in 32 days. It was observed that the silver leaching rates were high on the first day, which were then reduced drastically in the following days. After 12 days, the leaching rates of silver remained close

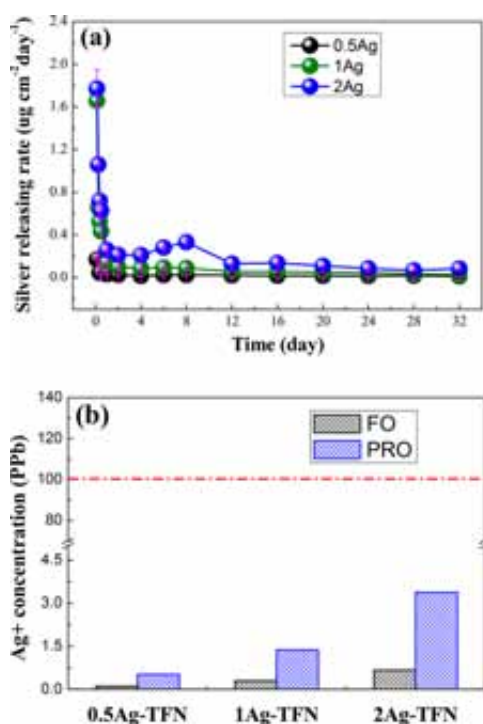


**Figure 11.** (a) Release rate of silver during 32 days leaching test; (b) the calculated Ag<sup>+</sup> concentration in draw solution under FO mode and in feed solution under PRO mode, respectively. The red dash line in (b) was the limited Ag<sup>+</sup> concentration (100 ppb) in drinking water according to WHO guidelines.

to zero, indicating that the silver ions were gradually released from the Ag/PAN-TFN FO membranes. On the other hand, with the increase of silver content in the Ag/PAN-TFN FO membrane, more silver ions were released.

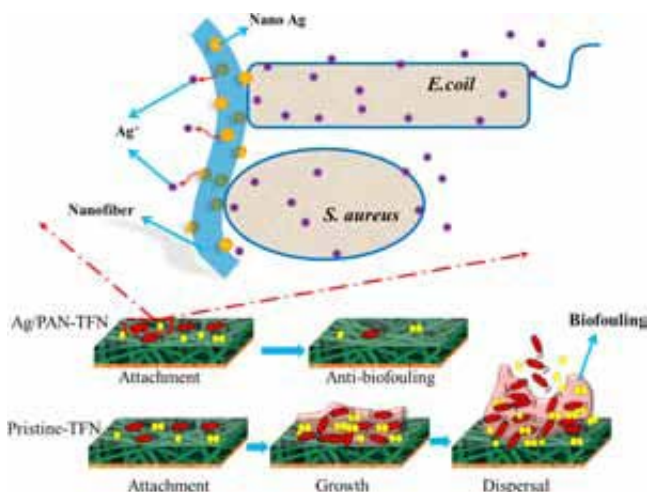
According to the percentages of AgNO<sub>3</sub> in the electro-spinning solution, the content of silver nanoparticles in the Ag/PAN-TFN FO membrane could be estimated. Based on calculation, after shaking in water for 32 days, the residual silver percentages were about 71%, 54%, and 49% for the 0.5Ag-TFN, 1Ag-TFN, and 2Ag-TFN FO membranes, respectively, relative to the corresponding pristine Ag/PAN-TFN FO membranes. Taking the average releasing rate from day 12 to day 32 to calculate, the silver ions would be continuously leached from the Ag/PAN-TFN FO membrane for more than one year if all the silver in the membranes could be completely released. It can be inferred that the AgNPs immobilized in the nanofibers acted as a silver ions reservoir and provided continuous antibacterial activity for the Ag/PAN-TFN FO membrane. This responded with the condition of inhibition zone and cell viability tests (Figures 8 and 9).

Figure 11b displays the Ag<sup>+</sup> concentration in the solution directly contacting the Ag/PAN-NFS layer of the different Ag/PAN-TFN FO membranes during a FO process. The Ag<sup>+</sup> concentration in the draw solution operated under FO mode and in the feed solution under PRO mode were calculated using eqs 3 and 4, respectively. In general, the silver ion concentration in feed solution under PRO mode will be higher than that in draw solution under FO mode. In PRO mode, the Ag/PAN-NFS faced the feed solution, and water was driven from the feed into the draw solution. Thus, the volume of feed solution gradually reduced, and the Ag<sup>+</sup> concentration in the feed increased more rapidly in the time frame. On the contrary, the Ag/PAN-NFS faced the draw solution in FO mode, under which water permeated into the draw solution. Therefore, compared to PRO mode, the Ag<sup>+</sup> concentration in the draw solution under FO mode was lower due to the increasing volume of the draw solution (Figure 11b).

For all Ag/PAN-TFN FO membranes, the amount of accumulated silver ions in water had a positive relationship with the content of silver, and the concentrations after 12 h were 3.38 ppb in feed solution under PRO mode and 0.67 ppb in draw solution under FO mode, respectively. It is worth noting that the limited concentration of silver in drinking water was 100 ppb according to the WHO guideline (2004). This demonstrated that the Ag/PAN-TFN FO membrane can be an appropriate antibiofouling and safe FO membrane.

The antibacterial mechanism of the Ag/PAN-TFN FO membranes was proposed and displayed in Figure 12. The silver ions could bond with organic amines, phosphates, and most notably thiols, forming a quasi-covalent bond.<sup>36</sup> On the other hand, there are abundant moieties in biological constituents such as cell wall, cell membrane, and DNA. Therefore, when the silver ions are released from the nanofiber support layer of the Ag/PAN-TFN FO membrane, some may be adsorbed readily to the lipopolysaccharide, proteins, and phospholipid on cell walls and cell membranes, causing the irreversible damage to the cell. Notably, some ions may penetrate through the cell wall, affecting ribosomal subunit proteins and some enzymes,<sup>37</sup> perturbing the structure of DNA, and ultimately resulting in cellular death.

As illustrated in Figure 12, in general, biofouling is formed through the deposition and attachment of microbial cells, followed by exopolymer production and cell growth, and the



**Figure 12.** Schematic diagram of the antibacterial mechanism of the Ag/PAN-TFN FO membrane.

dispersal of cells.<sup>13</sup> It is expected that the Ag/PAN-TFN FO membrane could eradicate most of the bacteria adherent on surface of the Ag/PAN-TFN layer, which shows good antibiofouling potential.

#### 4. CONCLUSIONS

TEM, XRD, and XPS analyses indicated that the monodisperse AgNPs with a diameter of about 10 nm were successfully incorporated into the PAN electrospun nanofiber mat via in situ synthesis. Having AgNPs tightly embedded in the nanofiber mat support, has improved hydrophilicity and antibacterial properties of the Ag/PAN-TFN FO membrane, leading to a bifunctional effect of both increased water flux and antibiofouling properties. With 0.5 M NaCl as the draw solution, the water flux of the Ag/PAN-TFN FO membrane could achieve 21.58 LMH and 29.21 LMH in FO and PRO modes, respectively. Leaching test showed that the AgNPs could act as a silver ions reservoir and slowly release silver ions into the solution, which endowed the Ag/PAN-TFN FO membranes with excellent antibacterial activity. The study suggested the AgNPs embedded electrospun PAN nanofiber mat could be applied as a promising support for antibiofouling FO membrane.

#### AUTHOR INFORMATION

##### Corresponding Author

\*Tel.: +86-592-6190785. E-mail: [ymzheng@iue.ac.cn](mailto:ymzheng@iue.ac.cn).

##### ORCID

Yu-Ming Zheng: 0000-0002-3858-1037

##### Notes

The authors declare no competing financial interest.

#### ACKNOWLEDGMENTS

The authors acknowledge the financial support received from the National Natural Science Foundation of China (Grant Nos. 51578525 and 5153000136), the Outstanding Youth Scientific Research Cultivation Plan Fujian Province University (2017, 147), and the Hundred Talents Program of Chinese Academy of Sciences.

#### REFERENCES

- (1) Elimelech, M.; Phillip, W. A. The future of seawater desalination: energy, technology, and the environment. *Science* **2011**, *333* (6043), 712–717.
- (2) Zhao, S. F.; Zou, L.; Tang, C. Y. Y.; Mulcahy, D. Recent developments in forward osmosis: Opportunities and challenges. *J. Membr. Sci.* **2012**, *396*, 1–21.
- (3) Xie, Z.; Hoang, M.; Duong, T.; Ng, D.; Dao, B.; Gray, S. Sol-gel derived poly(vinyl alcohol)/maleic acid/silica hybrid membrane for desalination by pervaporation. *J. Membr. Sci.* **2011**, *383* (1), 96–103.
- (4) Zhang, S.; Fu, F.; Chung, T.-S. Substrate modifications and alcohol treatment on thin film composite membranes for osmotic power. *Chem. Eng. Sci.* **2013**, *87*, 40–50.
- (5) Lu, T.-D.; Chen, B.-Z.; Wang, J.; Jia, T.-Z.; Cao, X.-L.; Wang, Y.; Xing, W.; Lau, C. H.; Sun, S.-P. Electrospun nanofiber substrates that enhance polar solvent separation from organic compounds in thin-film composites. *J. Mater. Chem. A* **2018**, *6* (31), 15047–15056.
- (6) Luo, W.; Phan, H. V.; Li, G.; Hai, F. I.; Price, W. E.; Elimelech, M.; Nghiem, L. D. An Osmotic Membrane Bioreactor–Membrane Distillation System for Simultaneous Wastewater Reuse and Seawater Desalination: Performance and Implications. *Environ. Sci. Technol.* **2017**, *51* (24), 14311–14320.
- (7) Zhao, X.; Li, J.; Liu, C. Improving the separation performance of the forward osmosis membrane based on the etched microstructure of the supporting layer. *Desalination* **2017**, *408*, 102–109.
- (8) Chen, Q.; Xu, W.; Ge, Q. Novel Multicharge Hydroacid Complexes That Effectively Remove Heavy Metal Ions from Water in Forward Osmosis Processes. *Environ. Sci. Technol.* **2018**, *52* (7), 4464–4471.
- (9) Pan, S. F.; Zhu, M. P.; Chen, J. P.; Yuan, Z. H.; Zhong, L. B.; Zheng, Y. M. Separation of tetracycline from wastewater using forward osmosis process with thin film composite membrane - Implications for antibiotics recovery. *Sep. Purif. Technol.* **2015**, *153*, 76–83.
- (10) Chowdhury, M. R.; Huang, L.; McCutcheon, J. R. Thin Film Composite Membranes for Forward Osmosis Supported by Commercial Nanofiber Nonwovens. *Ind. Eng. Chem. Res.* **2017**, *56* (4), 1057–1063.
- (11) Xu, S.; Lin, P.; An, X.; Hu, Y.; Wang, Z.; Zhong, L.; Niu, Q. High-Performance Forward Osmosis Membranes Used for Treating High-Salinity Oil-Bearing Wastewater. *Ind. Eng. Chem. Res.* **2017**, *56* (43), 12385–12394.
- (12) Xu, W.; Ge, Q. Novel functionalized forward osmosis (FO) membranes for FO desalination: Improved process performance and fouling resistance. *J. Membr. Sci.* **2018**, *555*, 507–516.
- (13) Matin, A.; Khan, Z.; Zaidi, S. M. J.; Boyce, M. C. Biofouling in reverse osmosis membranes for seawater desalination: Phenomena and prevention. *Desalination* **2011**, *281*, 1–16.
- (14) Mi, B. X.; Elimelech, M. Chemical and physical aspects of organic fouling of forward osmosis membranes. *J. Membr. Sci.* **2008**, *320* (1–2), 292–302.
- (15) Liu, Q.; Zhong, L.-B.; Zhao, Q.-B.; Frear, C.; Zheng, Y.-M. Synthesis of Fe<sub>3</sub>O<sub>4</sub>/Polyacrylonitrile Composite Electrospun Nanofiber Mat for Effective Adsorption of Tetracycline. *ACS Appl. Mater. Interfaces* **2015**, *7* (27), 14573–14583.
- (16) Nataraj, S. K.; Yang, K. S.; Aminabhavi, T. M. Polyacrylonitrile-based nanofibers—A state-of-the-art review. *Prog. Polym. Sci.* **2012**, *37* (3), 487–513.
- (17) Song, X. X.; Liu, Z. Y.; Sun, D. D. Energy recovery from concentrated seawater brine by thin-film nanofiber composite pressure retarded osmosis membranes with high power density. *Energy Environ. Sci.* **2013**, *6* (4), 1199–1210.
- (18) Pan, S.-F.; Dong, Y.; Zheng, Y.-M.; Zhong, L.-B.; Yuan, Z.-H. Self-sustained hydrophilic nanofiber thin film composite forward osmosis membranes: Preparation, characterization and application for simulated antibiotic wastewater treatment. *J. Membr. Sci.* **2017**, *523*, 205–215.

(19) Liu, L.; Liu, Z.; Bai, H.; Sun, D. D. Concurrent filtration and solar photocatalytic disinfection/degradation using high-performance Ag/TiO<sub>2</sub> nanofiber membrane. *Water Res.* **2012**, *46* (4), 1101–12.

(20) GhavamiNejad, A.; Rajan Unnithan, A.; Ramachandra Kurup Sasikala, A.; Samarikhalaj, M.; Thomas, R. G.; Jeong, Y. Y.; Nasser, S.; Murugesan, P.; Wu, D.; Hee Park, C.; Kim, C. S. Mussel-inspired electrospun nanofibers functionalized with size-controlled silver nanoparticles for wound dressing application. *ACS Appl. Mater. Interfaces* **2015**, *7* (22), 12176–12183.

(21) Huang, J.; Arthanareeswaran, G.; Zhang, K. Effect of silver loaded sodium zirconium phosphate (nanoAgZ) nanoparticles incorporation on PES membrane performance. *Desalination* **2012**, *285*, 100–107.

(22) Liu, X.; Qi, S.; Li, Y.; Yang, L.; Cao, B.; Tang, C. Y. Synthesis and characterization of novel antibacterial silver nanocomposite nanofiltration and forward osmosis membranes based on layer-by-layer assembly. *Water Res.* **2013**, *47* (9), 3081–3092.

(23) Ben-Sasson, M.; Lu, X.; Bar-Zeev, E.; Zodrow, K. R.; Nejati, S.; Qi, G.; Giannelis, E. P.; Elimelech, M. In situ formation of silver nanoparticles on thin-film composite reverse osmosis membranes for biofouling mitigation. *Water Res.* **2014**, *62* (0), 260–270.

(24) Le Ouay, B.; Stellacci, F. Antibacterial activity of silver nanoparticles: A surface science insight. *Nano Today* **2015**, *10* (3), 339–354.

(25) Wang, Y.; Yang, Q.; Shan, G.; Wang, C.; Du, J.; Wang, S.; Li, Y.; Chen, X.; Jing, X.; Wei, Y. Preparation of silver nanoparticles dispersed in polyacrylonitrile nanofiber film spun by electrospinning. *Mater. Lett.* **2005**, *59* (24–25), 3046–3049.

(26) Song, X.; Liu, Z.; Sun, D. D. Nano gives the answer: Breaking the bottleneck of internal concentration polarization with a nanofiber composite forward osmosis membrane for a high water production rate. *Adv. Mater.* **2011**, *23* (29), 3256–60.

(27) Huang, Z. M.; Zhang, Y. Z.; Kotaki, M.; Ramakrishna, S. A review on polymer nanofibers by electrospinning and their applications in nanocomposites. *Compos. Sci. Technol.* **2003**, *63* (15), 2223–2253.

(28) Kaspar, T. C.; Droubay, T.; Chambers, S. A.; Bagus, P. S. Spectroscopic evidence for Ag(III) in highly oxidized silver films by X-ray photoelectron spectroscopy. *J. Phys. Chem. C* **2010**, *114* (49), 21562–21571.

(29) Ferraria, A. M.; Carapeto, A. P.; Botelho do Rego, A. M. X-ray photoelectron spectroscopy: Silver salts revisited. *Vacuum* **2012**, *86* (12), 1988–1991.

(30) Chen, P.-C.; Wan, L.-S.; Xu, Z.-K. Bio-inspired CaCO<sub>3</sub> coating for superhydrophilic hybrid membranes with high water permeability. *J. Mater. Chem.* **2012**, *22* (42), 22727–22733.

(31) McCutcheon, J. R.; Elimelech, M. Influence of concentrative and dilutive internal concentration polarization on flux behavior in forward osmosis. *J. Membr. Sci.* **2006**, *284* (1–2), 237–247.

(32) Bui, N. N.; McCutcheon, J. R. Hydrophilic nanofibers as new supports for thin film composite membranes for engineered osmosis. *Environ. Sci. Technol.* **2013**, *47* (3), 1761–9.

(33) Huang, L.; McCutcheon, J. R. Hydrophilic nylon 6,6 nanofibers supported thin film composite membranes for engineered osmosis. *J. Membr. Sci.* **2014**, *457*, 162–169.

(34) Jung, W. K.; Koo, H. C.; Kim, K. W.; Shin, S.; Kim, S. H.; Park, Y. H. Antibacterial activity and mechanism of action of the silver ion in *Staphylococcus aureus* and *Escherichia coli*. *Appl. Environ. Microbiol.* **2008**, *74* (7), 2171–2178.

(35) Kim, S.; Ryu, D.-Y. Silver nanoparticle-induced oxidative stress, genotoxicity and apoptosis in cultured cells and animal tissues. *J. Appl. Toxicol.* **2013**, *33* (2), 78–89.

(36) Barngrover, B. M.; Aikens, C. M. Incremental binding energies of gold(I) and silver(I) thiolate clusters. *J. Phys. Chem. A* **2011**, *115* (42), 11818–11823.

(37) Yamanaka, M.; Hara, K.; Kudo, J. Bactericidal Actions of a Silver Ion Solution on *Escherichia coli*, Studied by Energy-Filtering Transmission Electron Microscopy and Proteomic Analysis. *Appl. Environ. Microbiol.* **2005**, *71* (11), 7589–7593.